

# Measurements of $J/\psi$ and $\psi(2S)$ decays into $\Lambda\bar{\Lambda}\pi^0$ and $\Lambda\bar{\Lambda}\eta$

M. Ablikim<sup>1</sup>, J. Z. Bai<sup>1</sup>, Y. Ban<sup>12</sup>, X. Cai<sup>1</sup>, H. F. Chen<sup>17</sup>, H. S. Chen<sup>1</sup>, H. X. Chen<sup>1</sup>, J. C. Chen<sup>1</sup>, Jin Chen<sup>1</sup>, Y. B. Chen<sup>1</sup>, Y. P. Chu<sup>1</sup>, Y. S. Dai<sup>19</sup>, L. Y. Diao<sup>9</sup>, Z. Y. Deng<sup>1</sup>, Q. F. Dong<sup>15</sup>, S. X. Du<sup>1</sup>, J. Fang<sup>1</sup>, S. S. Fang<sup>1a</sup>, C. D. Fu<sup>15</sup>, C. S. Gao<sup>1</sup>, Y. N. Gao<sup>15</sup>, S. D. Gu<sup>1</sup>, Y. T. Gu<sup>4</sup>, Y. N. Guo<sup>1</sup>, Z. J. Guo<sup>16b</sup>, F. A. Harris<sup>16</sup>, K. L. He<sup>1</sup>, M. He<sup>13</sup>, Y. K. Heng<sup>1</sup>, J. Hou<sup>11</sup>, H. M. Hu<sup>1</sup>, J. H. Hu<sup>3</sup>, T. Hu<sup>1</sup>, G. S. Huang<sup>1c</sup>, X. T. Huang<sup>13</sup>, X. B. Ji<sup>1</sup>, X. S. Jiang<sup>1</sup>, X. Y. Jiang<sup>5</sup>, J. B. Jiao<sup>13</sup>, D. P. Jin<sup>1</sup>, S. Jin<sup>1</sup>, Y. F. Lai<sup>1</sup>, G. Li<sup>1d</sup>, H. B. Li<sup>1</sup>, J. Li<sup>1</sup>, R. Y. Li<sup>1</sup>, S. M. Li<sup>1</sup>, W. D. Li<sup>1</sup>, W. G. Li<sup>1</sup>, X. L. Li<sup>1</sup>, X. N. Li<sup>1</sup>, X. Q. Li<sup>11</sup>, Y. F. Liang<sup>14</sup>, H. B. Liao<sup>1</sup>, B. J. Liu<sup>1</sup>, C. X. Liu<sup>1</sup>, F. Liu<sup>6</sup>, Fang Liu<sup>1</sup>, H. H. Liu<sup>1</sup>, H. M. Liu<sup>1</sup>, J. Liu<sup>12e</sup>, J. B. Liu<sup>1</sup>, J. P. Liu<sup>18</sup>, Jian Liu<sup>1</sup>, Q. Liu<sup>16</sup>, R. G. Liu<sup>1</sup>, Z. A. Liu<sup>1</sup>, Y. C. Lou<sup>5</sup>, F. Lu<sup>1</sup>, G. R. Lu<sup>5</sup>, J. G. Lu<sup>1</sup>, C. L. Luo<sup>10</sup>, F. C. Ma<sup>9</sup>, H. L. Ma<sup>2</sup>, L. L. Ma<sup>1f</sup>, Q. M. Ma<sup>1</sup>, Z. P. Mao<sup>1</sup>, X. H. Mo<sup>1</sup>, J. Nie<sup>1</sup>, S. L. Olsen<sup>16</sup>, R. G. Ping<sup>1</sup>, N. D. Qi<sup>1</sup>, H. Qin<sup>1</sup>, J. F. Qiu<sup>1</sup>, Z. Y. Ren<sup>1</sup>, G. Rong<sup>1</sup>, X. D. Ruan<sup>4</sup>, L. Y. Shan<sup>1</sup>, L. Shang<sup>1</sup>, C. P. Shen<sup>16</sup>, D. L. Shen<sup>1</sup>, X. Y. Shen<sup>1</sup>, H. Y. Sheng<sup>1</sup>, H. S. Sun<sup>1</sup>, S. S. Sun<sup>1</sup>, Y. Z. Sun<sup>1</sup>, Z. J. Sun<sup>1</sup>, X. Tang<sup>1</sup>, G. L. Tong<sup>1</sup>, G. S. Varner<sup>16</sup>, D. Y. Wang<sup>1g</sup>, L. Wang<sup>1</sup>, L. L. Wang<sup>1</sup>, L. S. Wang<sup>1</sup>, M. Wang<sup>1</sup>, P. Wang<sup>1</sup>, P. L. Wang<sup>1</sup>, W. F. Wang<sup>1h</sup>, Y. F. Wang<sup>1</sup>, Z. Wang<sup>1</sup>, Z. Y. Wang<sup>1</sup>, Zheng Wang<sup>1</sup>, C. L. Wei<sup>1</sup>, D. H. Wei<sup>1</sup>, Y. Weng<sup>1</sup>, N. Wu<sup>1</sup>, X. M. Xia<sup>1</sup>, X. X. Xie<sup>1</sup>, G. F. Xu<sup>1</sup>, X. P. Xu<sup>6</sup>, Y. Xu<sup>11</sup>, M. L. Yan<sup>17</sup>, H. X. Yang<sup>1</sup>, Y. X. Yang<sup>3</sup>, M. H. Ye<sup>2</sup>, Y. X. Ye<sup>17</sup>, G. W. Yu<sup>1</sup>, C. Z. Yuan<sup>1</sup>, Y. Yuan<sup>1</sup>, S. L. Zang<sup>1</sup>, Y. Zeng<sup>7</sup>, B. X. Zhang<sup>1</sup>, B. Y. Zhang<sup>1</sup>, C. C. Zhang<sup>1</sup>, D. H. Zhang<sup>1</sup>, H. Q. Zhang<sup>1</sup>, H. Y. Zhang<sup>1</sup>, J. W. Zhang<sup>1</sup>, J. Y. Zhang<sup>1</sup>, S. H. Zhang<sup>1</sup>, X. Y. Zhang<sup>13</sup>, Yiyun Zhang<sup>14</sup>, Z. X. Zhang<sup>12</sup>, Z. P. Zhang<sup>17</sup>, D. X. Zhao<sup>1</sup>, J. W. Zhao<sup>1</sup>, M. G. Zhao<sup>1</sup>, P. P. Zhao<sup>1</sup>, W. R. Zhao<sup>1</sup>, Z. G. Zhao<sup>1i</sup>, H. Q. Zheng<sup>12</sup>, J. P. Zheng<sup>1</sup>, Z. P. Zheng<sup>1</sup>, L. Zhou<sup>1</sup>, K. J. Zhu<sup>1</sup>, Q. M. Zhu<sup>1</sup>, Y. C. Zhu<sup>1</sup>, Y. S. Zhu<sup>1</sup>, Z. A. Zhu<sup>1</sup>, B. A. Zhuang<sup>1</sup>, X. A. Zhuang<sup>1</sup>, B. S. Zou<sup>1</sup>

(BES Collaboration)

<sup>1</sup> Institute of High Energy Physics, Beijing 100049, People's Republic of China

<sup>2</sup> China Center for Advanced Science and Technology (CCAST), Beijing 100080, People's Republic of China

<sup>3</sup> Guangxi Normal University, Guilin 541004, People's Republic of China

<sup>4</sup> Guangxi University, Nanning 530004, People's Republic of China

<sup>5</sup> Henan Normal University, Xinxiang 453002, People's Republic of China

<sup>6</sup> Huazhong Normal University, Wuhan 430079, People's Republic of China

<sup>7</sup> Hunan University, Changsha 410082, People's Republic of China

<sup>8</sup> Jinan University, Jinan 250022, People's Republic of China

<sup>9</sup> Liaoning University, Shenyang 110036, People's Republic of China

<sup>10</sup> Nanjing Normal University, Nanjing 210097, People's Republic of China

<sup>11</sup> Nankai University, Tianjin 300071, People's Republic of China

<sup>12</sup> Peking University, Beijing 100871, People's Republic of China

<sup>13</sup> Shandong University, Jinan 250100, People's Republic of China

<sup>14</sup> Sichuan University, Chengdu 610064, People's Republic of China

<sup>15</sup> Tsinghua University, Beijing 100084, People's Republic of China

<sup>16</sup> University of Hawaii, Honolulu, HI 96822, USA

<sup>17</sup> University of Science and Technology of China, Hefei 230026, People's Republic of China

<sup>18</sup> Wuhan University, Wuhan 430072, People's Republic of China

<sup>19</sup> Zhejiang University, Hangzhou 310028, People's Republic of China

<sup>a</sup> Current address: DESY, D-22607, Hamburg, Germany

<sup>b</sup> Current address: Johns Hopkins University, Baltimore, MD 21218, USA

<sup>c</sup> Current address: University of Oklahoma, Norman, Oklahoma 73019, USA

<sup>d</sup> Current address: Universite Paris XI, LAL-Bat. 208-BP34, 91898 ORSAY Cedex, France

<sup>e</sup> Current address: Max-Planck-Institut fuer Physik, Foehringer Ring 6, 80805 Munich, Germany

<sup>f</sup> Current address: University of Toronto, Toronto M5S 1A7, Canada

<sup>g</sup> Current address: CERN, CH-1211 Geneva 23, Switzerland

<sup>h</sup> Current address: Laboratoire de l'Accélérateur Linéaire, Université Paris-Sud 11, Bâtiment 208, BP34, 91898 Orsay, France

<sup>i</sup> Current address: University of Michigan, Ann Arbor, MI 48109, USA

(Dated: February 14, 2013)

Using 58 million  $J/\psi$  and 14 million  $\psi(2S)$  events collected by the BESII detector at the BEPC,

branching fractions or upper limits for the decays  $J/\psi$  and  $\psi(2S) \rightarrow \Lambda\bar{\Lambda}\pi^0$  and  $\Lambda\bar{\Lambda}\eta$  are measured. For the isospin violating decays, the upper limits are determined to be  $\mathcal{B}(J/\psi \rightarrow \Lambda\bar{\Lambda}\pi^0) < 6.4 \times 10^{-5}$  and  $\mathcal{B}(\psi(2S) \rightarrow \Lambda\bar{\Lambda}\pi^0) < 4.9 \times 10^{-5}$  at the 90% confidence level. The isospin conserving process  $J/\psi \rightarrow \Lambda\bar{\Lambda}\eta$  is observed for the first time, and its branching fraction is measured to be  $\mathcal{B}(J/\psi \rightarrow \Lambda\bar{\Lambda}\eta) = (2.62 \pm 0.60 \pm 0.44) \times 10^{-4}$ , where the first error is statistical and the second one is systematic. No  $\Lambda\bar{\Lambda}\eta$  signal is observed in  $\psi(2S)$  decays, and  $\mathcal{B}(\psi(2S) \rightarrow \Lambda\bar{\Lambda}\eta) < 1.2 \times 10^{-4}$  is set at the 90% confidence level. Branching fractions of  $J/\psi$  decays into  $\Sigma^+\pi^-\bar{\Lambda}$  and  $\bar{\Sigma}^-\pi^+\Lambda$  are also reported, and the sum of these branching fractions is determined to be  $\mathcal{B}(J/\psi \rightarrow \Sigma^+\pi^-\bar{\Lambda} + c.c.) = (1.52 \pm 0.08 \pm 0.16) \times 10^{-3}$ .

PACS numbers: 13.25.Gv, 12.38.Qk, 14.20.Gk, 14.40.Cs

## I. INTRODUCTION

Several charmonium decay modes containing  $\Lambda\bar{\Lambda}$  pairs have been reported [1, 2, 3, 4, 5, 6, 7, 8]. Among these decays, the isospin violating process  $J/\psi \rightarrow \Lambda\bar{\Lambda}\pi^0$  has been studied by DM2 [3] and BESII [4], and its average branching fraction is determined to be  $\mathcal{B}(J/\psi \rightarrow \Lambda\bar{\Lambda}\pi^0) = (2.2 \pm 0.6) \times 10^{-4}$  [9]. However, the isospin conserving process  $J/\psi \rightarrow \Lambda\bar{\Lambda}\eta$  has not been reported, and there are no measurements for  $\Lambda\bar{\Lambda}\pi^0$  and  $\Lambda\bar{\Lambda}\eta$  decays of  $\psi(2S)$ .

In this paper, we study  $J/\psi$  and  $\psi(2S) \rightarrow \Lambda\bar{\Lambda}\pi^0$ ,  $\Lambda\bar{\Lambda}\eta$  using 58 M  $J/\psi$  events and 14 M  $\psi(2S)$  events taken with the BESII detector at the BEPC storage ring. We find that the  $J/\psi \rightarrow \Lambda\bar{\Lambda}\pi^0$  branching fraction is much smaller than those measured by DM2 and BESII. In addition, we observe the isospin conserving process  $J/\psi \rightarrow \Lambda\bar{\Lambda}\eta$  and measure its branching fraction for the first time. Analyses of  $\Lambda\bar{\Lambda}\pi^0$  and  $\Lambda\bar{\Lambda}\eta$  in  $\psi(2S)$  decays are also performed, but no obvious signals are observed for these two channels.

## II. THE BESII DETECTOR AND MONTE CARLO SIMULATION

BESII is a conventional solenoidal magnet detector that is described in detail in Ref. [10]. A 12-layer vertex chamber (VTC) surrounding the beam pipe provides trigger and track information. A forty-layer main drift chamber (MDC), located radially outside the VTC, provides trajectory and energy loss ( $dE/dx$ ) information for charged tracks over 85% of the total solid angle. The momentum resolution is  $\sigma_p/p = 0.0178\sqrt{1+p^2}$  ( $p$  in GeV/c), and the  $dE/dx$  resolution for hadron tracks is  $\sim 8\%$ . An array of 48 scintillation counters surrounding the MDC measures the time-of-flight (TOF) of charged tracks with a resolution of  $\sim 200$  ps for hadrons. Radially outside the TOF system is a 12 radiation length, lead gas-tube barrel shower counter (BSC). This measures the energies of electrons and photons over  $\sim 80\%$  of the total solid angle with an energy resolution of  $\sigma_E/E = 21\%/\sqrt{E}$  ( $E$  in GeV). Outside of the solenoidal coil, which provides a 0.4 Tesla magnetic field over the tracking volume, is an iron flux return that is instrumented with three double layers of counters that identify muons of momentum

greater than 0.5 GeV/c.

In this analysis, a GEANT3 based Monte Carlo (MC) simulation program [11] with detailed consideration of real detector responses (such as dead electronic channels) is used. The consistency between data and Monte Carlo has been carefully checked in many high-purity physics channels, and the agreement is quite reasonable [12].

## III. EVENT SELECTION

The decay channels investigated in this paper are  $J/\psi \rightarrow \Lambda\bar{\Lambda}\pi^0$ ,  $J/\psi \rightarrow \Lambda\bar{\Lambda}\eta$ ,  $\psi(2S) \rightarrow \Lambda\bar{\Lambda}\pi^0$ , and  $\psi(2S) \rightarrow \Lambda\bar{\Lambda}\eta$ , where  $\Lambda$  decays to  $\pi^-p$  and  $\pi^0$  and  $\eta$  to  $\gamma\gamma$ . The final states in which we are interested contain two photons and four charged tracks ( $\pi^+\pi^-\bar{p}p$ ). Candidate events are required to satisfy the following common selection criteria:

1. Events must have four good charged tracks with net charge zero. A good charged track is a track that is well fitted to a helix in the MDC and has a polar angle,  $\theta$ , in the range  $|\cos\theta| < 0.8$ .
2. The TOF and  $dE/dx$  measurements of the charged tracks are used to calculate  $\chi^2_{PID}$  values for the hypotheses that the particle is a pion, kaon, or proton. Only the two proton tracks must be identified with the requirement that  $\chi^2_{PID}$  for the proton hypothesis is less than those for the  $\pi$  or  $K$  hypotheses.
3. Isolated photons are those that have an energy deposit in the BSC greater than 50 MeV and have the angle between the photon entering the BSC, and the shower development direction in the BSC less than  $37^\circ$ . In order to remove the fake photons produced by  $\bar{p}$  annihilation and those produced by hadronic interactions of tracks with the shower counter, the angle between the photon and antiproton is required to be larger than  $25^\circ$  and those between the photon and other charged tracks larger than  $8^\circ$ .
4. The selected events are subjected to four constraint (4C) kinematic fits. When there are more than two candidate photons in an event, all combinations are

tried and the combination with the smallest  $\chi_{4C}^2$  is retained. The selection requirement on  $\chi_{4C}^2$  is optimized by maximizing  $S/\sqrt{S+B}$ , where  $S$  and  $B$  are the expected numbers of signal and background events, respectively.

5. To select  $\Lambda$  and  $\bar{\Lambda}$ , the difference between the measured  $\pi p$  mass and the expected mass ( $M(\Lambda)$ ) should be less than  $10 \text{ MeV}/c^2$  (three times the  $\Lambda$  mass resolution).

#### IV. EVENT ANALYSIS

##### A. $J/\psi \rightarrow \Lambda \bar{\Lambda} \pi^0$

###### 1. Event Selection

Only events with two good photons are selected, and 4C kinematic fits under the  $\gamma\gamma\pi^+\pi^-p\bar{p}$  hypothesis are performed. To select clean  $\Lambda\bar{\Lambda}$  events, we require the  $\Lambda$  and  $\bar{\Lambda}$  secondary vertices to be reconstructed successfully, and the decay lengths of  $\Lambda$  and  $\bar{\Lambda}$  in the  $x-y$  plane must be larger than  $0.05 \text{ m}$ .

Figure 1 shows the  $\Lambda\bar{\Lambda}$  invariant mass ( $M(\Lambda\bar{\Lambda})$ ) distribution after the above selection. The large peak near  $2.9 \text{ GeV}/c^2$  is background from  $J/\psi \rightarrow \Sigma^0\bar{\Sigma}^0$ , in agreement with the expectation from the MC simulation, normalized to its branching fraction [9], shown as the shaded histogram in Fig. 1. To reject such background,  $M(\Lambda\bar{\Lambda})$  is required to be less than  $2.8 \text{ GeV}/c^2$ . With this selection, Fig. 2 shows the  $\chi_{4C}^2$  distribution for data and Monte

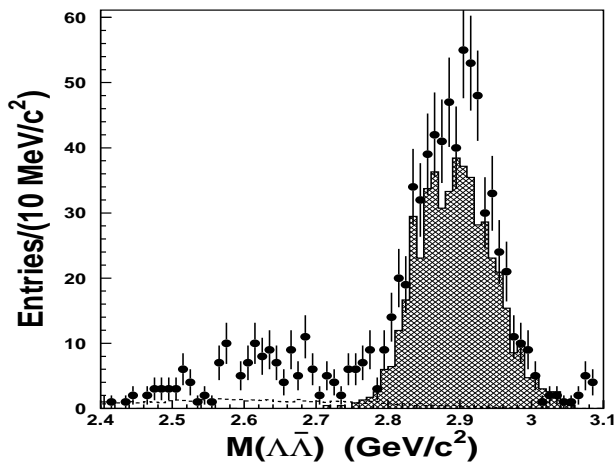


FIG. 1: Distribution of  $M(\Lambda\bar{\Lambda})$  for  $J/\psi \rightarrow \Lambda\bar{\Lambda}\gamma\gamma$  candidates. Dots with error bars are data, the shaded histogram is background from MC simulated  $J/\psi \rightarrow \Sigma^0\bar{\Sigma}^0$ , normalized according to the branching fraction in the PDG, and the dashed histogram is the MC simulated  $J/\psi \rightarrow \Lambda\bar{\Lambda}\pi^0$  signal, normalized according to the branching fraction in the PDG.

Carlo simulation. To suppress potential backgrounds,  $\chi_{4C}^2 < 10$  is required.

###### 2. Background Analysis

To explore other possible backgrounds, we generate MC events for the following channels:  $J/\psi \rightarrow \gamma\Lambda\bar{\Lambda}$ ,  $\Sigma^0\bar{\Sigma}^0$ ,  $\Sigma(1385)^0\bar{\Sigma}(1385)^0$ ,  $\Xi^0\bar{\Xi}^0$ ,  $\Xi(1530)^0\bar{\Xi}^0$ ,  $\Sigma^0\pi^0\bar{\Lambda} + c.c.$ , and  $\Sigma^+\pi^-\bar{\Lambda} + c.c.$ . Only the last two channels give significant contributions to the  $\pi^0$  signal. In particular, the decay mode  $J/\psi \rightarrow \Sigma^0\pi^0\bar{\Lambda} + c.c.$ , which contains  $\Lambda\bar{\Lambda}\pi^0$  with an additional photon in the final state, could contribute to the observed number of  $\Lambda\bar{\Lambda}\pi^0$  candidates. Because direct measurements of  $J/\psi \rightarrow \Sigma^0\pi^0\bar{\Lambda} + c.c.$  are difficult, we measure the branching fractions of their isospin partners and estimate their branching fractions by assuming isospin symmetry. To estimate the contamination from  $J/\psi \rightarrow \Sigma^0\pi^0\bar{\Lambda} + c.c.$ , a high precision measurement of  $J/\psi \rightarrow \Sigma^+\pi^-\bar{\Lambda} + c.c.$  is very important.

###### 3. Measurement of $J/\psi \rightarrow \Sigma^+\pi^-\bar{\Lambda} + c.c.$

The  $J/\psi \rightarrow \Sigma^+\pi^-\bar{\Lambda} + c.c.$  events, where  $\Sigma^+ \rightarrow \pi^0 p$  and  $\bar{\Lambda} \rightarrow \pi^+\bar{p}$ , have the same final states as the signal channel  $\Lambda\bar{\Lambda}\pi^0$ . Candidate events are required to satisfy  $\chi_{4C}^2 < 15$ , in addition to the common selection criteria in Section III, except for the  $\Lambda$  and  $\bar{\Lambda}$  mass requirements. Figure 3 is a scatter plot of  $M(\pi^+\bar{p})$  versus  $M(\pi^-p)$  invariant mass for data and MC simulation. The two bands are the  $J/\psi \rightarrow \Sigma^+\pi^-\bar{\Lambda} + c.c.$  events. In order to select  $J/\psi \rightarrow \Sigma^+\pi^-\bar{\Lambda}$ ,  $M(\pi^-p) > 1.15 \text{ GeV}/c^2$  is required. Figure 4 shows the scatter plot of  $M(\gamma\gamma)$  versus  $M(\pi^+\bar{p})$ . The intersection region (central box) of the  $\pi^0$  and  $\bar{\Lambda}$  bands corresponds

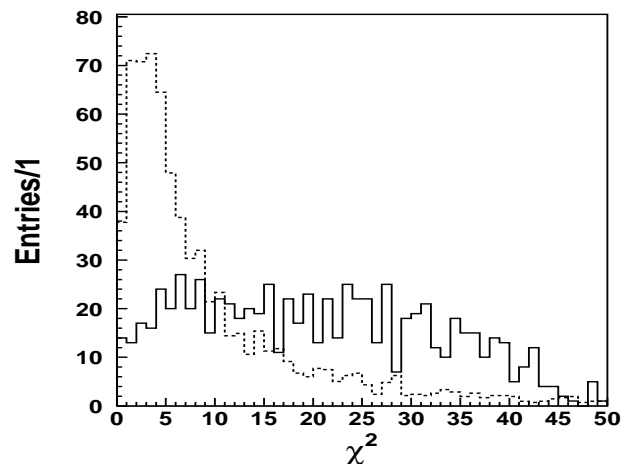


FIG. 2: Distribution of  $\chi_{4C}^2$  for  $J/\psi \rightarrow \Lambda\bar{\Lambda}\gamma\gamma$  candidate events (solid histogram) and Monte Carlo simulated  $J/\psi \rightarrow \Lambda\bar{\Lambda}\pi^0$  events (dashed histogram). Here,  $M(\Lambda\bar{\Lambda})$  is required to be less than  $2.8 \text{ GeV}/c^2$ .

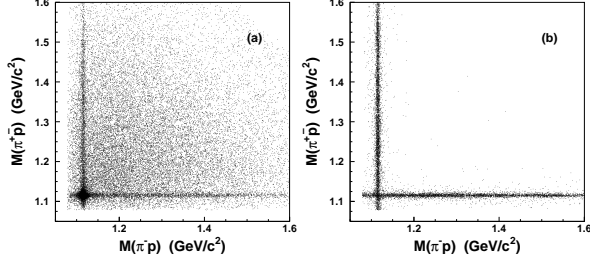


FIG. 3: Scatter plot of  $M(\pi^+\bar{p})$  versus  $M(\pi^-p)$  invariant mass for (a)  $J/\psi \rightarrow \Sigma^+\pi^-\bar{\Lambda}$  (+c.c.) candidate events and (b) MC simulation.

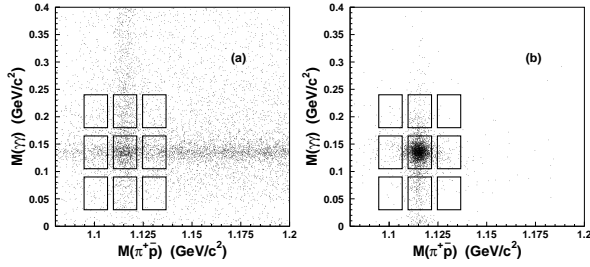


FIG. 4: Scatter plot of  $M(\gamma\gamma)$  versus  $M(\pi^+\bar{p})$  for (a)  $J/\psi \rightarrow \Sigma^+\pi^-\bar{\Lambda}$  candidate events and (b) MC simulation of  $J/\psi \rightarrow \Sigma^+\pi^-\bar{\Lambda}$ , both satisfying  $\chi^2_{4C} < 15$ . The central box in the figure is the signal region defined by  $|M(\gamma\gamma) - M(\pi^0)| < 0.03$   $\text{GeV}/c^2$  and  $|M(\pi^+\bar{p}) - M(\bar{\Lambda})| < 0.006$   $\text{GeV}/c^2$ . The  $\pi^0$  sideband is defined by  $|M(\gamma\gamma) - 0.06| < 0.03$   $\text{MeV}/c^2$  and  $|M(\gamma\gamma) - 0.21| < 0.03$   $\text{GeV}/c^2$  (The two boxes located above and below the signal region), and the  $\bar{\Lambda}$  sideband region by  $|M(\pi^+\bar{p}) - 1.101| < 0.006$   $\text{GeV}/c^2$  and  $|M(\pi^+\bar{p}) - 1.131| < 0.006$   $\text{GeV}/c^2$  (The two boxes on the left and right of the signal region). The four boxes at the corners are used to estimate the phase space contribution.

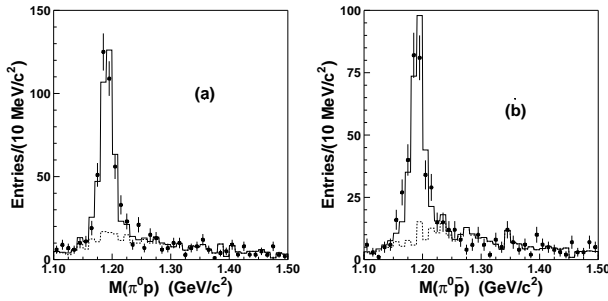


FIG. 5: (a)  $M(\pi^0 p)$  of  $J/\psi \rightarrow \pi^0 p \pi^-\bar{\Lambda}$  candidate events from the signal region of Fig. 4 and (b)  $M(\pi^0 \bar{p})$  of  $J/\psi \rightarrow \pi^0 \bar{p} \pi^+ \Lambda$  candidate events. Dots with error bars are data, the solid histograms are the best fits described in the text, and the dashed histograms are backgrounds estimated from  $\Lambda$  and  $\pi^0$  sidebands.

to the  $J/\psi \rightarrow \Sigma^+\pi^-\bar{\Lambda}$  signal. The dots with error bars in Fig. 5 (a) show the distribution of  $M(\pi^0 p)$  invariant mass of the events in the central box ( $|M(\gamma\gamma) - M(\pi^0)| < 30$   $\text{MeV}/c^2$  and  $|M(\pi^+\bar{p}) - M(\bar{\Lambda})| < 6$   $\text{MeV}/c^2$ ), and a clear  $\Sigma^+$  signal is observed. The dashed histogram is the background coming from sidebands of  $\pi^0$  and  $\bar{\Lambda}$ . To obtain the number of  $\Sigma^+$  events, we fit the  $\Sigma^+$  signal with a histogram of the signal shape from MC simulation plus the background shape determined from the  $\pi^0$  and  $\bar{\Lambda}$  sidebands.  $335 \pm 22$   $\Sigma^+$  events are obtained from the fit. We do a similar analysis to measure  $J/\psi \rightarrow \bar{\Sigma}^-\pi^+\Lambda$ . The signal for  $\bar{\Sigma}^-$  and the fitting result are shown in Fig. 5 (b). The fit yields  $254 \pm 19$  events.

The efficiencies for  $J/\psi \rightarrow \Sigma^+\pi^-\bar{\Lambda}$  and  $J/\psi \rightarrow \bar{\Sigma}^-\pi^+\Lambda$  are determined to be 2.3% and 1.8% using  $2 \times 10^5$  MC simulated signal events, respectively. The branching fractions are calculated to be  $\mathcal{B}(J/\psi \rightarrow \Sigma^+\pi^-\bar{\Lambda}) = (7.70 \pm 0.51) \times 10^{-4}$  and  $\mathcal{B}(J/\psi \rightarrow \bar{\Sigma}^-\pi^+\Lambda) = (7.47 \pm 0.56) \times 10^{-4}$ , where the errors are statistical. The total branching fraction of the two conjugate modes is  $\mathcal{B}(J/\psi \rightarrow \Sigma^+\pi^-\bar{\Lambda} + \text{c.c.}) = (15.17 \pm 0.76) \times 10^{-4}$ .

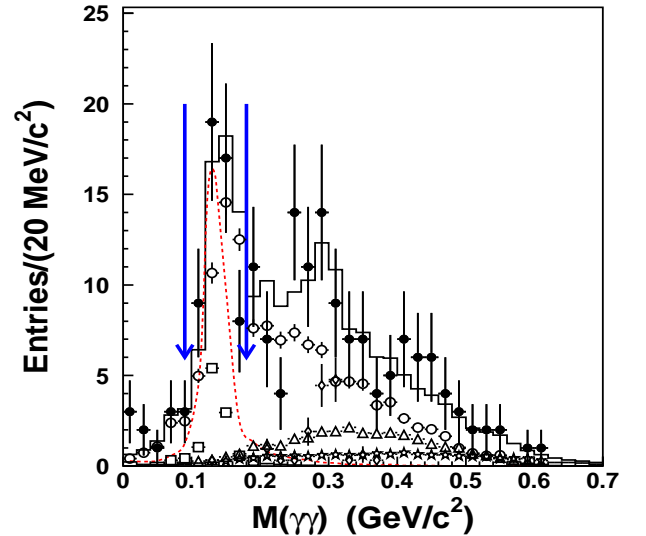


FIG. 6: Invariant mass distribution of  $M(\gamma\gamma)$  for  $J/\psi \rightarrow \Lambda\bar{\Lambda}\gamma\gamma$  candidates (dots with error bars) and normalized backgrounds (solid histogram). The dashed curves shows the  $\pi^0$  signal from MC simulated  $J/\psi \rightarrow \Lambda\bar{\Lambda}\pi^0$ . The arrows denote the region of the  $\pi^0$  signal defined in the text. We use different histogram styles to indicate leading backgrounds from  $J/\psi \rightarrow \Sigma^0\pi^0\bar{\Lambda}$  (+c.c.) (circles),  $J/\psi \rightarrow \Sigma^+\pi^-\bar{\Lambda}$  (+c.c.) (squares),  $J/\psi \rightarrow \Xi^0\Xi^0$  (triangles),  $J/\psi \rightarrow \Sigma(1385)^0\bar{\Sigma}(1385)^0$  (stars) and  $J/\psi \rightarrow \Sigma^0\bar{\Sigma}^0$  (rhombi), which contribute  $46.0 \pm 5.4$ ,  $11.2 \pm 1.3$ ,  $1.9 \pm 0.4$ ,  $1.0 \pm 0.3$ , and 0 events in the defined  $\pi^0$  region.

#### 4. Background determination and upper limit on the number of signal events

Using the branching fractions for  $J/\psi \rightarrow \Sigma^+ \pi^- \bar{\Lambda} + c.c.$  measured above and branching fractions available in the PDG [9], we obtain 29.2, 14.3, 14.2, 125.0, and 11.9 background events from  $J/\psi \rightarrow \Xi^0 \bar{\Xi}^0$ ,  $J/\psi \rightarrow \Sigma^0 \bar{\Sigma}^0$ ,  $J/\psi \rightarrow \Sigma(1385)^0 \bar{\Sigma}(1385)^0$ ,  $J/\psi \rightarrow \Sigma^0 \pi^0 \bar{\Lambda} (+c.c.)$ , and  $J/\psi \rightarrow \Sigma^+ \pi^- \bar{\Lambda} (+c.c.)$  for the  $J/\psi \rightarrow \Lambda \bar{\Lambda} \pi^0$  selection, respectively. We also studied backgrounds from other possible channels listed in the PDG [9] that might contaminate the  $\pi^0$  signal, but their contamination was found to be negligible. The histogram in Fig. 6 shows normalized backgrounds from all background channels. The normalized  $M(\gamma\gamma)$  distribution of the background events is in reasonable agreement with the data. The dashed line in the figure shows the  $\pi^0$  signal from MC simulated  $J/\psi \rightarrow \Lambda \bar{\Lambda} \pi^0$ . To estimate the expected number of signal events, we define the  $\pi^0$  mass region as  $|M(\gamma\gamma) - M(\pi^0)| < 0.045 \text{ GeV}/c^2$ , which is indicated in the figure and selects most of the  $\pi^0$  signal events. The numbers of  $\pi^0$  events in the mass region are found to be  $54.0 \pm 7.4$  and  $60.1 \pm 9.5$  for data and normalized backgrounds, respectively. By using the POLE method [13, 14], the upper limit on the number of  $\pi^0$  events from  $J/\psi \rightarrow \Lambda \bar{\Lambda} \pi^0$  is calculated to be 11.2 at the 90% confidence level (C.L.).

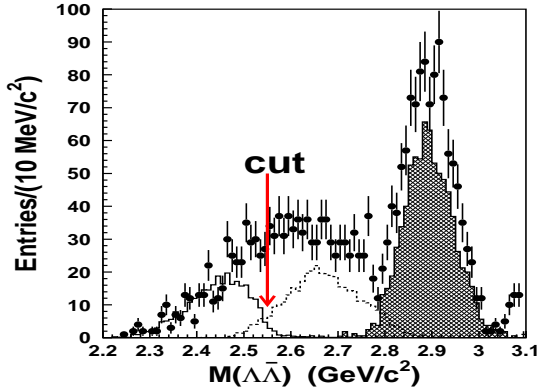


FIG. 7: The  $\Lambda\bar{\Lambda}$  invariant mass distribution for  $J/\psi \rightarrow \Lambda\bar{\Lambda}\gamma\gamma$  candidates (dots with error bars), background from MC simulated  $J/\psi \rightarrow \Sigma^0\bar{\Sigma}^0$  (hatched histogram), background from MC simulated  $J/\psi \rightarrow \Xi^0\bar{\Xi}^0$  (dashed histogram), and MC simulated  $J/\psi \rightarrow \Lambda\bar{\Lambda}\eta$  signal (solid histogram). The backgrounds are normalized according to the branching fractions in the PDG and the  $\Lambda\bar{\Lambda}\eta$  signal is normalized using the branching fraction measured in this paper. The arrow indicates the  $M(\Lambda\bar{\Lambda})$  requirement, and events below the arrow are selected as  $J/\psi \rightarrow \Lambda\bar{\Lambda}\eta$  candidates.

#### B. $J/\psi \rightarrow \Lambda\bar{\Lambda}\eta$

Candidate events with two or three good photons are selected, and the  $\chi^2_{4C}$  is required to be less than 15. Since the momenta of  $\Lambda$  and  $\bar{\Lambda}$  are low in this channel, no requirement is made on the decay lengths of  $\Lambda$  and  $\bar{\Lambda}$ ; otherwise the efficiency would be extremely low. This is demonstrated in Fig. 6, where a decay length requirement is made and no  $\eta$  signal is seen. Figure 7 shows the  $\Lambda\bar{\Lambda}$  invariant mass distribution after the above selection. To remove the backgrounds from  $J/\psi \rightarrow \Sigma^0\bar{\Sigma}^0$  and  $J/\psi \rightarrow \Xi^0\bar{\Xi}^0$ , events with  $M(\Lambda\bar{\Lambda}) > 2.55 \text{ GeV}/c^2$  are rejected, since for the signal process, they are kinematically prohibited. Dots with error bars in Fig. 8 show the invariant mass of  $M(\gamma\gamma)$ , and a clear  $\eta$  signal is observed.

To investigate possible backgrounds, we consider the following channels with  $\Lambda$  or  $\Xi$  production:  $J/\psi \rightarrow \gamma\Lambda\bar{\Lambda}$ ,  $\Sigma^0\bar{\Sigma}^0$ ,  $\Sigma(1385)^0\bar{\Sigma}(1385)^0$ ,  $\Xi^0\bar{\Xi}^0$ ,  $\Xi(1530)^0\bar{\Xi}^0$ ,  $\Sigma^0\pi^0\bar{\Lambda} + c.c.$ , and  $\Sigma^+\pi^-\bar{\Lambda} + c.c.$ . Using available branching fractions of these decay modes, we obtain 7.8, 27.6, 6.2, and 20.4 background events from  $J/\psi \rightarrow \Xi^0\bar{\Xi}^0$ ,  $J/\psi \rightarrow \Sigma(1385)^0\bar{\Sigma}(1385)^0$ ,  $J/\psi \rightarrow \Xi(1530)^0\bar{\Xi}^0$ , and  $\Sigma^0\pi^0\bar{\Lambda} + c.c.$  in the mass region  $M(\gamma\gamma) > 0.4 \text{ GeV}/c^2$ , respectively. The background contribution from the  $\Lambda\bar{\Lambda}$  sidebands ( $|M(\pi p) - 1.141| < 0.01 \text{ GeV}/c^2$ ) is evaluated to be  $3 \pm 2$  events. Contamination from other possible channels listed in the PDG [9] that might contaminate the  $\eta$  signal is negligible. The shaded histogram in Fig. 8 shows the normalized backgrounds from the above channels. We fit the  $\gamma\gamma$  invariant mass distribution with a MC simulated signal shape and a second order polynomial background. The fit yields  $44 \pm 10$  events with a statistical significance of  $4.8\sigma$ .

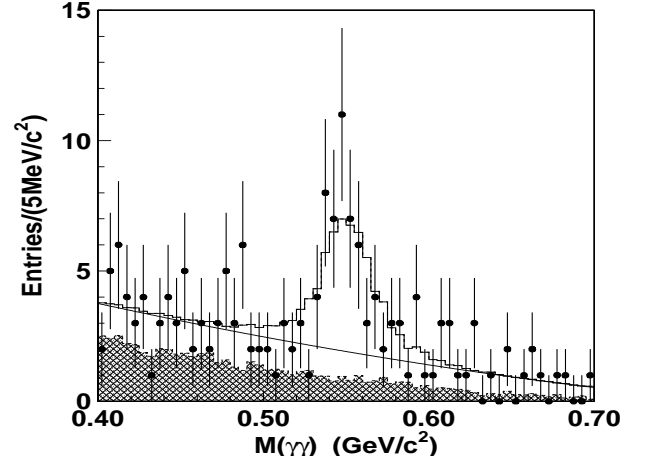


FIG. 8: Fit to the  $\gamma\gamma$  invariant mass distribution of  $J/\psi \rightarrow \Lambda\bar{\Lambda}\gamma\gamma$  candidate events selected in Fig. 7. Dots with error bars are data, the hatched histogram is the normalized background from all the channels considered, and the solid histogram is the fit to data using a histogram of the signal shape from MC simulation plus a second order polynomial for background.

### C. $\psi(2S) \rightarrow \Lambda \bar{\Lambda} \pi^0$ and $\Lambda \bar{\Lambda} \eta$

The selection criteria for these two decays are similar to those for  $J/\psi$  decays. A 4C kinematic fit to the hypothesis  $\psi(2S) \rightarrow \gamma\gamma\pi^+\pi^-p\bar{p}$  for candidate events with two good photons is performed, and the  $\chi^2_{4C}$  is required to be less than 15. Backgrounds from  $\psi(2S) \rightarrow \pi^+\pi^-J/\psi$  are rejected with the requirement  $|M_{\pi^+\pi^-}^{recoil} - M(J/\psi)| > 0.04$   $\text{GeV}/c^2$ , where  $M_{\pi^+\pi^-}^{recoil}$  is the recoiling mass of  $\pi^+\pi^-$ . Figure 9 (d) depicts the invariant mass distribution of the charged tracks. The peak around  $3.1 \text{ GeV}/c^2$  is from  $\psi(2S) \rightarrow \text{neutral} + J/\psi$ . In order to veto such background,  $|M(\Lambda\bar{\Lambda}) - M(J/\psi)| > 0.05 \text{ GeV}/c^2$  is required. Furthermore, to suppress the background from  $\psi(2S) \rightarrow \Sigma^0\bar{\Sigma}^0$  shown in Fig. 9, the invariant mass of  $\Lambda\bar{\Lambda}$  is required to be less than  $3.3 \text{ GeV}/c^2$ .

Figure 10 shows the  $\gamma\gamma$  invariant mass distribution after the above selection, and we see no significant  $\pi^0$  or  $\eta$  signals. In order to estimate the number of signal events, we define the signal regions as  $0.09 < M(\gamma\gamma) < 0.18$  and  $0.50 < M(\gamma\gamma) < 0.60$  ( $\text{GeV}/c^2$ ) for  $\pi^0$  and  $\eta$ , respectively. The number of signal events is found to be 4 in both regions. To estimate the backgrounds from the sidebands of  $\pi^0$  and  $\eta$ ,  $(0.03 - 0.08)$  and  $(0.19 - 0.25)$  ( $\text{GeV}/c^2$ ) are taken as the sidebands of  $\pi^0$ , and  $(0.43 - 0.49)$ ,  $(0.61 - 0.67)$  ( $\text{GeV}/c^2$ ) are taken as the sidebands of  $\eta$ . The numbers of background events from the sidebands of  $\pi^0$  and  $\eta$  are estimated to be 1 and 1.5. With the POLE method [13, 14], the upper limits on the numbers of signal events at the 90% C.L. are calculated to be 7.0 and 7.6, respectively.

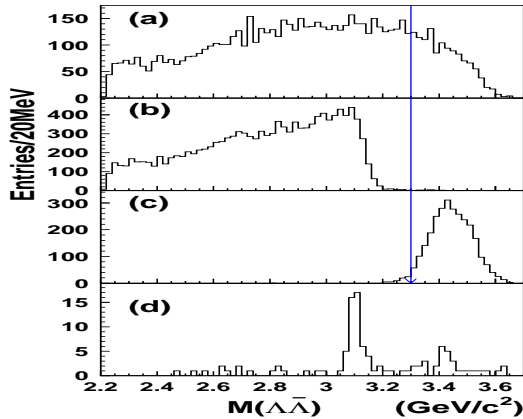


FIG. 9:  $M(\Lambda\bar{\Lambda})$  distribution for MC simulated events: (a)  $\psi(2S) \rightarrow \Lambda\bar{\Lambda}\pi^0$ , (b)  $\psi(2S) \rightarrow \Lambda\bar{\Lambda}\eta$ , and (c)  $\psi(2S) \rightarrow \Sigma^0\bar{\Sigma}^0$ . (d) The  $M(\Lambda\bar{\Lambda})$  distribution for data. The arrow denotes the selection  $M(\Lambda\bar{\Lambda}) < 3.3 \text{ GeV}/c^2$ .

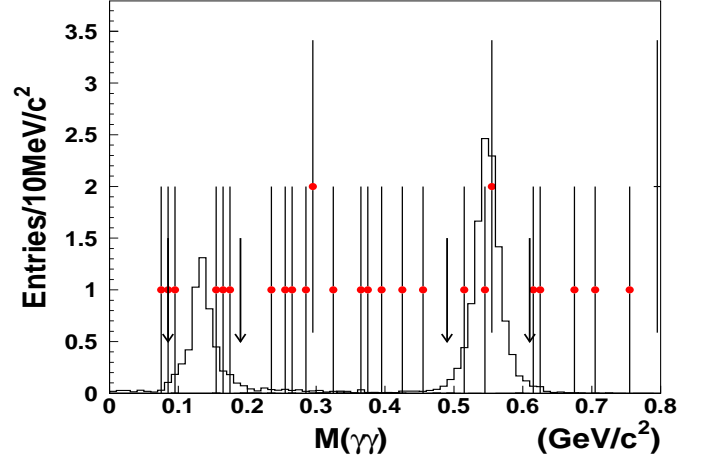


FIG. 10: The  $\gamma\gamma$  invariant mass distribution for candidate  $\psi(2S) \rightarrow \gamma\gamma\Lambda\bar{\Lambda}$  events. Dots with error bars are data, and the histograms are MC simulated signal events. The arrows indicate the signal region of  $\pi^0$  and  $\eta$  described in the text.

### V. SYSTEMATIC ERRORS

The systematic errors on the branching fractions are mainly from the efficiency differences between data and MC simulation in the MDC tracking, particle identification (PID), photon detection, kinematic fitting, the  $\Lambda$  vertex finding, and the decay length requirement and the uncertainties on the total number of  $J/\psi$  and  $\psi(2S)$  events.

The MDC tracking and particle identification (PID) systematic errors are estimated from the difference of the selection efficiencies of protons and antiprotons between data and MC simulation [15]. The efficiencies are measured using samples of  $J/\psi \rightarrow \pi^+\pi^-p\bar{p}$  and  $\psi(2S) \rightarrow \pi^+\pi^-p\bar{p}$ , which are selected using PID for three tracks, allowing one proton or antiproton at a time to be missing in the fit [15]. The efficiency difference between data and MC simulation for one proton is from 2% to 5% depending on the proton momentum of the decay channels.

The photon detection efficiency is studied using  $J/\psi \rightarrow \rho^0\pi^0$  in Ref. [16]. The results indicate that the systematic error is about 2% for each photon. Therefore, 4% is taken as the systematic error on the photon efficiency for all the decays.

The uncertainty due to the kinematic fit is studied using many channels which can be selected purely without a kinematic fit [15, 16, 17]. It is found that the MC simulates the kinematic fit efficiency at the 5% level for almost all channels tested. Therefore, we take 5% as the systematic error due to the kinematic fit.

The  $\Lambda$  reconstruction systematic errors are studied using  $J/\psi \rightarrow \Lambda\bar{\Lambda}$  [7, 8]. The  $\Lambda$  secondary vertex finding gives a systematic error of 0.7% for each  $\Lambda$  vertex, and the decay length requirement contributes 1.7%. The total percentage error arising from  $\Lambda$  and  $\bar{\Lambda}$  vertex require-

TABLE I: Summary of systematic errors (%).

Source	$J/\psi \rightarrow \Lambda \bar{\Lambda} \pi^0$	$J/\psi \rightarrow \Lambda \bar{\Lambda} \eta$	$\psi(2S) \rightarrow \Lambda \bar{\Lambda} \pi^0$	$\psi(2S) \rightarrow \Lambda \bar{\Lambda} \eta$	$J/\psi \rightarrow \Sigma^+ \pi^- \bar{\Lambda}$	$J/\psi \rightarrow \bar{\Sigma}^- \pi^+ \Lambda$
Tracking and PID	7.0	14.0	6.0	12.0	7.0	6.0
Photon efficiency	4.0	4.0	4.0	4.0	4.0	4.0
Kinematic fit	5.0	5.0	5.0	5.0	5.0	5.0
$\Lambda$ vertex requirement	3.7	-	-	-	-	-
Background shape	-	3.0	-	-	2.2	1.5
Number of good photons	3.0	3.0	3.0	3.0	-	-
Total number of events	4.7	4.7	4.0	4.0	4.7	4.7
Total	11.6	16.6	10.1	14.5	10.8	10.1

TABLE II: Measured branching fractions or upper limits at 90% confidence level (C.L.) for all the studied channels. Here,  $\mathcal{B}(\Lambda \rightarrow \pi^- p) = 63.9\%$ ,  $\mathcal{B}(\Sigma^+ \rightarrow \pi^0 p) = 51.6\%$  and  $\mathcal{B}(\eta \rightarrow \gamma\gamma) = 39.4\%$  are taken from the PDG.

Channels	Number of events	MC efficiency(%)	Branching fraction ( $\times 10^{-4}$ )
$J/\psi \rightarrow \Lambda \bar{\Lambda} \pi^0$	$< 11.2$	0.75	$< 0.64$
$J/\psi \rightarrow \Lambda \bar{\Lambda} \eta$	$44 \pm 10$	1.8	$2.62 \pm 0.60 \pm 0.44$
$\psi(2S) \rightarrow \Lambda \bar{\Lambda} \pi^0$	$< 7.0$	2.5	$< 0.49$
$\psi(2S) \rightarrow \Lambda \bar{\Lambda} \eta$	$< 7.6$	2.9	$< 1.2$
$J/\psi \rightarrow \Sigma^+ \pi^- \bar{\Lambda}$	$335 \pm 22$	2.3	$7.70 \pm 0.51 \pm 0.83$
$J/\psi \rightarrow \bar{\Sigma}^- \pi^+ \Lambda$	$254 \pm 19$	1.8	$7.47 \pm 0.56 \pm 0.76$
$J/\psi \rightarrow \Sigma^+ \pi^- \bar{\Lambda} + c.c.$			$15.17 \pm 0.76 \pm 1.59$

ments is 3.7%.

The systematic error of the background shape can be determined by fitting the observed  $\Sigma^+$ ,  $\bar{\Sigma}^-$  and  $\eta$  signal events with different background shapes. For  $J/\psi \rightarrow \Sigma^+ \pi^- \bar{\Lambda}$  and  $J/\psi \rightarrow \bar{\Sigma}^- \pi^+ \Lambda$ , the background shape in fitting the  $\Sigma^+$  and  $\bar{\Sigma}^-$  is changed to a second order polynomial. The differences in the numbers of fitted  $\Sigma^+$  and  $\bar{\Sigma}^-$  events are found to be 2.2% and 1.5%, respectively. For  $J/\psi \rightarrow \Lambda \bar{\Lambda} \eta$ , the background shape is changed from a second order polynomial to a first order one, and the difference in the number of fitted signal events is about 3%.

The uncertainty caused by the requirement of two good photons is estimated by considering the percentage of events without fake photons in the sample of  $J/\psi \rightarrow \Lambda \bar{\Lambda}$ . It is found that the difference in the percentages of events without fake photons between data and MC simulation is 3%, which is taken as the systematic error for the requirement of two good photons.

Finally, the results reported here are based on a total of 58 M  $J/\psi$  events and 14 M  $\psi(2S)$  events. The uncertainties on the number of  $J/\psi$  and  $\psi(2S)$  events are 4.7% and 4.0%, respectively. Table I lists the systematic errors from all sources. Adding all errors in quadrature, the total percentage errors range from 10% to 17% for all the studied decay channels.

## VI. RESULTS AND DISCUSSION

Table II lists the results for  $J/\psi$  and  $\psi(2S)$  decay into  $\Lambda \bar{\Lambda} \pi^0$  and  $\Lambda \bar{\Lambda} \eta$ , as well as  $J/\psi \rightarrow \Sigma^+ \pi^- \bar{\Lambda} + c.c.$ . We also list the total branching fraction for the conjugate modes, where the common systematic errors have been taken out. Except for  $J/\psi \rightarrow \Lambda \bar{\Lambda} \pi^0$  and  $J/\psi \rightarrow \Sigma^+ \pi^- \bar{\Lambda} + c.c.$ , the results are first measurements. Interestingly, the result of  $J/\psi \rightarrow \Lambda \bar{\Lambda} \pi^0$  presented here is much smaller than those of DM2 and BES1 [3, 4]. In previous experiments, the large contaminations from  $J/\psi \rightarrow \Sigma^0 \pi^0 \bar{\Lambda} + c.c.$  and  $J/\psi \rightarrow \Sigma^+ \pi^- \bar{\Lambda} + c.c.$  were not considered, resulting in a large value of branching fraction for  $J/\psi \rightarrow \Lambda \bar{\Lambda} \pi^0$ . The small branching fraction of  $J/\psi \rightarrow \Lambda \bar{\Lambda} \pi^0$  and relatively large branching fraction of  $J/\psi \rightarrow \Lambda \bar{\Lambda} \eta$  measured here indicate that the isospin violating decay in  $J/\psi$  decays is suppressed while isospin conserving decays are favored, which is consistent with expectation.

## VII. ACKNOWLEDGMENT

The BES collaboration thanks the staff of BEPC and computing center for their hard efforts. This work is supported in part by the National Natural Science Foundation of China under contracts Nos. 10491300, 10225524,

10225525, 10425523, 10625524, 10521003, the Chinese Academy of Sciences under contract No. KJ 95T-03, the 100 Talents Program of CAS under Contract Nos. U-11, U-24, U-25, and the Knowledge Innovation Project of CAS under Contract Nos. U-602, U-34 (IHEP), U-

612(IHEP), the National Natural Science Foundation of China under Contract Nos. 10225522, 10491305 (Tsinghua University), MOE of China under contract No. IRT0624 (CCNU), and the Department of Energy under Contract No. DE-FG02-04ER41291 (U. Hawaii).

- 
- [1] MarkI Collaboration, I. Peruzzi *et al.*, Phys. Rev. D **17**, 2901 (1978).
  - [2] MarkII Collaboration, M. W. Eaton *et al.*, Phys. Rev. D **29**, 804 (1984).
  - [3] DM2 Collaboration, P. Henrard *et al.*, Nucl. Phys. B **292**, 670 (1987).
  - [4] BES Collaboration, J. Z. Bai *et al.*, Phys. Lett. B **424**, 213 (1998).
  - [5] BES Collaboration, J. Z. Bai *et al.*, Phys. Rev. D **63**, 032002 (2001).
  - [6] CLEO Collaboration, T. K. Pedlar *et al.*, Phys. Rev. D **72**, 051108 (2005).
  - [7] BES Collaboration, M. Ablikim *et al.*, Phys. Lett. B **632**, 181 (2006).
  - [8] BES Collaboration, M. Ablikim *et al.*, Phys. Lett. B **648**, 149 (2007).
  - [9] Particle Physics Group, W. M. Yao *et al.*, J. Phys. G **33**, 1 (2006).
  - [10] BES Collaboration, J. Z. Bai *et al.*, Nucl. Inst. Meths. A **458**, 627 (2001).
  - [11] CERN Application Software Group, GEANT Detector Description and Simulation Tool, CERN Program Library Long Writeup W 5013, Geneva(1994).
  - [12] BES Collaboration, M. Ablikim *et al.*, Nucl. Inst. Meths. A **552**, 344 (2005).
  - [13] J. Conrad *et al.*, Phys. Rev. D **67**, 012002 (2003).
  - [14] Y. S. Zhu, Nucl. Inst. Meths. A **578**, 322 (2007).
  - [15] BES Collaboration, M. Ablikim *et al.*, Phys. Rev. D **71**, 072006 (2005).
  - [16] BES Collaboration, J. Z. Bai *et al.*, Phys. Rev. D **70**, 012005 (2004).
  - [17] BES Collaboration, J. Z. Bai *et al.*, Phys. Rev. D **69**, 092001 (2004).